Mechanics of Materials 217 (2026) 105656

Contents lists available at ScienceDirect

Mechanics of Materials

journal homepage: www.elsevier.com/locate/mecmat

Research paper

The full-field coverage characterization over the energy domain of hyperelastic isotropic materials

Federico O. Falope *

DIEF, Department of Engineering "Enzo Ferrari", via Pietro Vivarelli 10, 41125 Modena, Italy
National Group of Mathematical Physics (GNFM-INdAM), FIM UNIMORE, Via G. Campi, 213/A, 41125 Modena, Italy
Inter-departmental research and innovation centre on construction and environmental services, CRICT, via P. Vivarelli 10, 41125 Modena, Italy

ARTICLE INFO

Keywords:
Hyperelasticity
Isotropic materials
Two-dimensional characterization
Strain energy
Design biaxial tests
Strain invariants
Kinematic paths

ABSTRACT

In this work, the mechanical characterization of hyperelastic materials is critically reframed by presenting the full-field coverage characterization of the constitutive response of a material. We shift the focus from the experimental tests to the kinematic paths they trace over the energy domain, and from the measured stresses to the corresponding combinations of derivatives of the strain energy function. The key features of the full-field coverage characterization include the use of a single unequal biaxial experiment, the ability to reconstruct the effective response function of the material using simple equilibrium relations, and the coverage of the entire domain of the strain energy function. Conducting multiple experimental tests is costly. The standard tests, such as simple tension/compression, simple shear, and equi-biaxial tests, are not suited for characterizing the strain energy, as they only explore a single and limited kinematic path within the energy domain. For incompressible materials, the strain energy and its derivatives form surfaces on the stretches or strain invariants domain, which should be explicitly visualized using experiments. This two-dimensional nature is often overlooked and it is fundamentally reconsidered here. The *analogy of a mountain relief surveyed by a terrestrial drone* is proposed to highlight the often-overlooked two-dimensional nature of incompressible materials behavior. In silico simulations, based on a known energy function and constitutive parameters, are used to generate an "experimental" dataset to evaluate the proposed procedure. The results of the full-field coverage characterization introduce a novel paradigm that more accurately reproduces the behavior of soft materials than the simultaneous fitting of standard tests.

1. Introduction

One of the primary challenges in predicting the mechanical response of materials undergoing large deformations is capturing the form of their strain energy (Signorini, 1930; Truesdell, 1956; Signorini, 1959). Achieving this exactly would entail predicting any mechanical phenomenon with unprecedented accuracy. In doing this, it seems necessary to describe the strain energy function of the material. However, the real key lies in the *derivatives of the energy function* (DEF) for the deformation invariants, whose combinations yield the material response functions (Truesdell, 1952; Baker and Ericksen, 1954; Beatty, 1987), and whose further combinations determine the stress state of the material. Measuring the stress response of a material subjected to an experiment and deriving its constitutive law is the goal of the mechanical characterization.

Typically, the mechanical characterization process primarily requires a form of the strain energy, which, for hyperelastic and isotropic materials, is expressed as a symmetric function of the stretches or as a function of the deformation invariants. Regardless of the variables chosen to represent the energy, the energy function includes a set of scalar quantities that define the constitutive parameters of the material. Once the energy form is assumed, simple experimental tests—uniaxial tension/compression, equi-biaxial tension, or simple shear (Rivlin and Saunders, 1951; Treloar, 1944)—or more complex tests (Crocker et al., 1999; Brieu et al., 2007; Meunier et al., 2008) are carried out to create a starting point for the fitting procedure of the constitutive parameters. A common feature of most of these tests is the availability of a closed-form analytical solution, which enables a practical fitting of experimental data. The fitting procedure (Ogden et al., 2004; Steinmann et al., 2012), by minimizing the distance between the experimental data and the analytic model, provides the best-fit constitutive parameters of the material model.

* Correspondence to: DIEF, Department of Engineering "Enzo Ferrari", via Pietro Vivarelli 10, 41125 Modena, Italy.
E-mail address: fefalope@unimore.it.

https://doi.org/10.1016/j.mechmat.2026.105656
Received 8 October 2025; Received in revised form 1 December 2025; Accepted 3 March 2026
Available online 6 March 2026

A *non-standard characterization* is understood as a methodology that either employs non-standard experiments (beyond uniaxial, equi-biaxial, or simple shear tests) or, given experimental data, operates directly on the energy function of the tested material. Non-standard characterization is beginning to gain traction within the scientific community. This trend reflects a growing recognition that the standard experiments used to identify or fit constitutive parameters are affected by significant limitations. Recent works (Leygue et al., 2018; Costecalde et al., 2023) have presented procedures for identifying the strain-stress relation in non-linear elastic materials without relying on a predefined constitutive equation. The strength of these approaches, which combine data-driven identification algorithms with a single non-trivial experiment, lies in their ability to operate directly on the strain energy of the material. The use of a single test, albeit non-homogeneous, is an innovative and promising feature. However, the complex inhomogeneous deformation involved in such tests prevents a direct analytical formulation of the problem. In addition, the data-driven identification entails a significant computational cost, which is further compounded by the subsequent fitting procedure. Notable conceptual advances in non-standard characterization have been introduced by Prasad and Kannan (2020) and Kulwant et al. (2023). These authors propose a semi-analytical method for reconstructing the energy function by directly working with it and its derivatives. However, the required test—a combined tension/compression and simple shear test—is not straightforward to replicate, especially in terms of the effective prescribed stresses at the boundary and homogeneous deformations induced.

To date, the *standard characterization* presents three important limitations:

1. the lack of any type of verification or control over the effective behavior of each DEF. This is because the quality of the fitting is assessed exclusively based on the stresses, which in turn depend on specific combinations of DEF. Falope et al. (2024a) have shown that the uniaxial and equi-biaxial tests, as well as the typical experimental set-up of simple shear, do not allow for the assessment of all the DEF, and are therefore energetically unexhaustive or partially exhaustive. The outcomes of the fitting procedure on such tests cannot be checked. Yet, these remain the most commonly used experiments for mechanical characterization.
2. the reliability of the constitutive parameters improves when the fitting procedure is performed on multiple tests simultaneously. However, conducting more tests requires additional time and a significant financial investment for the acquisition of experimental devices.
3. multiple sets of constitutive parameters can reproduce the same response function (Ogden et al., 2004; Steinmann et al., 2012).

The objective of the following work is to overcome the first two limitations and mitigate the third one, thus laying the foundations for a new modus operandi for material characterization. We propose to conduct the characterization process using a single and simple test capable of visualizing and obtaining the DEF. The unique feature of this test, which we will demonstrate to be a particular unequal biaxial test, is to supply information about the material across its entire energy domain.

The work is organized as follows. Section 2 reviews the analytical preliminaries required to obtain the functions used to enhance the foundation of the mechanical characterization. Section 3 presents the standard fitting procedure. Then, through the analogy of the survey of a mountain relief, we introduce the rationale and analytical side of the experimental protocol for the new characterization process, called the *full-field coverage* (FFC) characterization. Built on the foundation of the FFC characterization, Section 4 presents an application of the protocol, demonstrating its potential through in silico experiments. Discussion and conclusion are drawn in Sections 5 and 6.

2. Analytic preliminaries

This section presents the analytical preliminaries for characterizing isotropic materials. Attention is paid to the choice of the deformation measure, as this choice may or may not permit the tracing of the DEF.

When hyperelastic materials are modeled as isotropic and incompressible, the strain energy density $W = W(I_1, I_2)$[1] is a two-dimensional function of some deformation invariants, I_1 and I_2, which are scalar functions of the principal stretches λ_i, derived from the deformation gradient $\mathbf{F}$. These invariants are arbitrarily chosen as a function of a strain measure, which defines how the deformation is quantified in formulating the problem.

We consider two deformation measures: the Henchy strain tensor $\boldsymbol{\eta} = \log \mathbf{V}$, which is associated with the left stretch tensor $\mathbf{V}$, and the widely used left Cauchy–Green deformation tensor $\mathbf{C} = \mathbf{F}^{\mathrm{T}}\mathbf{F}$. For incompressible materials, a plausible choice of principal invariants of these deformation measures could be K_{i+1} and I_i $(i = 1, 2)$ (Criscione et al., 2000; Rivlin and Saunders, 1951), defined as

$$K_2 = \sqrt{\operatorname{tr}\left(\boldsymbol{\eta}\boldsymbol{\eta}^{\mathrm{T}}\right)}, \quad K_3 = 3\sqrt{6}\det(\boldsymbol{\eta}/K_2), \tag{1a}$$

$$I_1 = \operatorname{tr}\mathbf{C}, \quad I_2 = \left(I_1^2 - \operatorname{tr}\mathbf{C}^2\right)/2. \tag{1b}$$

The two strain measures and their invariants are related to the logarithm and the squares of the principal stretches, $\boldsymbol{\eta}$ and $\mathbf{C}$ respectively.

The strain energy function serves as a bridge between kinematics and mechanics through a representation theorem. For the two choices of invariants, the first Piola–Kirchhoff stress tensor is

$$\mathbf{P} = \frac{\partial W}{\partial \boldsymbol{\eta}}\mathbf{F}^{-\mathrm{T}} = -p\mathbf{F}^{-\mathrm{T}} + \left(W_{K_2}\boldsymbol{\Phi} + \frac{W_{K_3}}{K_2}\mathbf{Y}\right)\mathbf{F}^{-\mathrm{T}}, \tag{2a}$$

$$\mathbf{P} = \frac{\partial W}{\partial \mathbf{F}} = -p\mathbf{F}^{-\mathrm{T}} + 2\left(W_1\mathbf{B} - W_2\mathbf{B}^{-1}\right)\mathbf{F}^{-\mathrm{T}}, \tag{2b}$$

where $\boldsymbol{\Phi} = \boldsymbol{\eta}/K_2$, $\mathbf{Y} = 3\sqrt{6}\boldsymbol{\Phi}^2 - \sqrt{6}\mathbf{I} - 3K_3\boldsymbol{\Phi}$, $\mathbf{B} = \mathbf{F}\,\mathbf{F}^{\mathrm{T}}$, and p is the hydrostatic pressure to be determined using boundary conditions. The DEF are W_{K_i} and W_i in the Criscione and Cauchy invariants formulations, respectively. The nominal stress tensor assumes the following explicit form:

$$\mathbf{P}_{ii} = \frac{1}{\lambda_i}K_2^3\Big[-K_2^2\left(K_2 p + \sqrt{6}W_{K_3}\right) + K_2\log\lambda_i\Big(K_2 W_{K_2} - 3K_3 W_{K_3}\Big) + 3\sqrt{6}\,W_{K_3}\log^2\lambda_i\Big], \tag{3a}$$

$$\mathbf{P}_{ii} = -\frac{p}{\lambda_i} + 2\lambda_i W_1 - \frac{2W_2}{\lambda_i^3}, \tag{3b}$$

being $\lambda_1\lambda_2\lambda_3 = 1$. When deformations are homogeneous, the stress tensor is also homogeneous and fulfills the indefinite equilibrium conditions. Boundary conditions $\mathbf{P}\,\mathbf{n} = \mathbf{s}$, being $\mathbf{n}$ the normal unit vector at the boundary and $\mathbf{s}$ the vector of the applied pressure, enclose the equilibrium problem. From relations (3), it is evident that the stress measures depends on the combination of DEF. It is more restrictive to work on the characterization of DEF, or at least consider them in the characterization, than to judge the quality of the fitting by observing only the entire stress response. These are the analytic preliminaries for the characterization of hyperelastic incompressible materials.

3. Characterization of hyperelastic isotropic materials

In this section, we first present how hyperelastic materials are typically characterized and then, through the analogy of the survey of a mountain relief, we propose a new approach for the 2D or 3D characterization of materials. We introduce the difference between the standard characterization and the *FFC* characterization.

[1] We focus on the case of incompressible material. However, as briefly recalled in the following sections, the rationale of the procedure can also be applied to compressible materials. We recall also that the energy can be formulated in terms of stretches (Ogden, 1972) or invariants.

3.1. Standard fitting procedure of the energy using one or multiple experiments

In the case of homogeneous deformations, the Piola–Kirchhoff stress tensor (3) and the boundary conditions of the test provide any stress component measured during the experiments. Let us for instance consider the kinematics of uniaxial tension, where $\lambda_1 = \lambda_2 = 1/\lambda^{1/2}$ and $\lambda_3 = \lambda \geq 1$. Using relation (3) and boundary conditions ($\bar{s}_3 = \bar{s}$ and $\bar{s}_1 = \bar{s}_2 = 0$)[2] , the analytic expression of the non-vanishing stress component follows straightforwardly

$$\bar{s}(\lambda) = \sqrt{\frac{3}{2}}\frac{W_{K_2}}{\lambda}, \tag{4a}$$

$$\bar{s}(\lambda) = \frac{2\left(\lambda^3 - 1\right)\left(\lambda W_1 + W_2\right)}{\lambda^3}. \tag{4b}$$

The experiments provide the stress vs. stretches curve, which, by means of a fitting procedure, represents the discrete form of (4). At this point, one of the *biggest problems of mathematical-physics* (Signorini, 1959) arises: the choice of an appropriate form of the energy W able to reproduce the experimental data. The energy form is univocally identified when its constitutive parameters are fixed. This is the goal of the fitting procedure. By a minimization process of an established objective function, it identifies the constitutive parameters of the assumed strain energy function. We define $\mathbf{p}$ as the optimal set of constitutive parameters. It is identified by looking at $\min_{\bar{\bar{\mathbf{p}}}} \text{obj}(\mathbf{p})$. The objective function is composed of the normalized root mean squared error,

$$\text{NRMSE}(x,\, f,\, \mathbf{p}) = \sqrt{\frac{\sum_i (f_i^{ex} - f_i^{an})^2}{\sum_i (f_i^{ex})^2}},$$

where $f_i^{an} = f^{an}(x_i)$ is the value of the analytical model sampled at the data points x_i and f_i^{ex} denotes the experimental value. In the case of multiple experiments, the objective function includes as many NRMSE terms as there are experiments. In contrast, for a single experiment, the NRMSE directly corresponds to the objective function. This is the standard simultaneous fitting of multiple states of stress summarized in Fig. 1. The enhancement points introduced by the FFC characterization are treated in the next section.

3.2. Full-field coverage (FFC) characterization over the entire domain

Before delving into the analytical and experimental details of the new modus operandi outlined in Fig. 1, we introduce the analogy of the mountain survey, which helps clarify the rationale behind the FFC characterization.

A topographic survey can be interpreted as the systematic sampling of a scalar field over a two-dimensional domain in order to reconstruct its topology. Each measurement corresponds to the evaluation of the field — such as height in the case of a topographic survey, or energy and its derivatives in the subsequent figurative example — at specific coordinates, enabling interpolation and the identification of gradients, extrema, and curvature across the domain.

In a topographic survey conducted on the ground by a terrestrial drone, the field values are sampled exclusively along the path traveled. Therefore, the path design and the sampling density along it determine how accurately the two-dimensional field is described. Particular attention should thus be paid to both the spatial distribution of the sampling points within the domain and their density. Accordingly, the expression *full-field coverage* is used to indicate that the proposed procedure achieves a comprehensive sampling of the strain energy domain, thereby covering the field in its entirety rather than along isolated deformation paths.

[2] From now on, the over-bar and double over-bar symbols denote the uniaxial and biaxial reactive stresses, respectively.

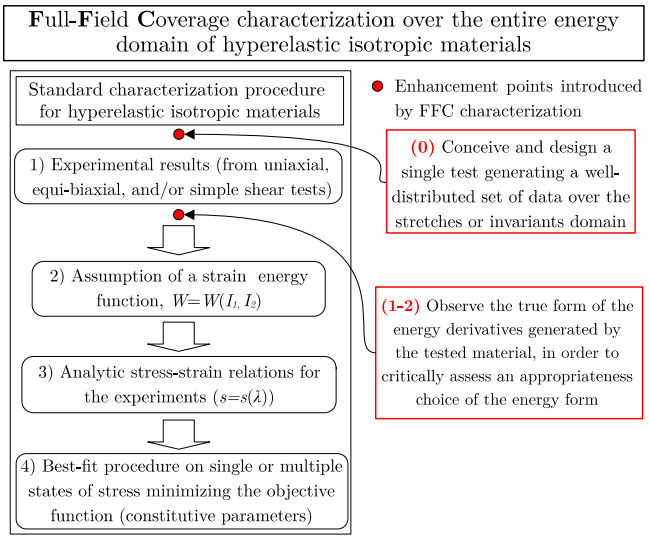

Fig. 1. Schedule of the standard characterization process and the additional enhancement points (in red) introduced by the full-field coverage (FFC) characterization. (For interpretation of the references to color in this figure legend, the reader is referred to the web version of this article.)

3.2.1. The survey of a mountain relief as the material characterization: The analogy

An operator conducts a topographic survey of the mountain relief shown in Fig. 2(a) using a terrestrial drone. The drone is controlled via a remote control operating in the reference system $O\lambda_1\lambda_2$ of Fig. 2(b). The drone measures the altitude of the mountain relative to an arbitrary reference system rather than the remote control reference system. The operator must first plan the drone path within the arbitrary reference system to best map the mountain surface.

Two arbitrary reference systems are shown in Figs. 2(c) and (d), corresponding to the coordinates system $K_2 - K_3$ and $I_1 - I_2$, respectively. Assume that the remote command is subject to alteration, resulting in a nonlinear motion of the drone within the arbitrary reference systems. Thus, a non-trivial mapping exists between the remote control reference system $O\lambda_1\lambda_2$ and the arbitrary reference systems $K_2 - K_3$ and $I_1 - I_2$. The boundaries of the arbitrary reference systems are shown using blue and cyan lines in Figs. 2(c), (d), and (e). Insurmountable barriers are erected along these lines. The drone cannot operate beyond these boundaries. This is the same scenario as in the characterization process of hyperelastic, incompressible, and isotropic materials.

The remote reference system of the drone represents the principal stretches domain, while the arbitrary reference systems correspond to two different choices of the invariants. The drone motion represents an experimental setup, with different motions corresponding to different experimental tests. The surface of the mountain represents the energy or a DEF.

The mapping between the reference systems, which are the command and the arbitrary ones, depends on the choice of the strain invariants. It is non-trivial (see relations (1)), as it is not a one-to-one analytic relation, except for permutation of the stretches (Rivlin and Sawyers, 1976; Rivlin, 2004; Currie, 2005; Anssari-Benam et al., 2024; Horgan and Murphy, 2025). Experimentally, this implies that different experimental paths in the stretches domain may correspond to the same path in the invariants space. This is because the symmetry of the invariants with respect to the stretches is not influenced by a permutation of the stretches.

Regardless of the path set remotely, the drone can move exclusively between the blue and cyan lines in Figs. 2(c), (d), and (e). The two choices of arbitrary reference systems exhibit different boundaries due to the distinct mappings from the remote control reference system.

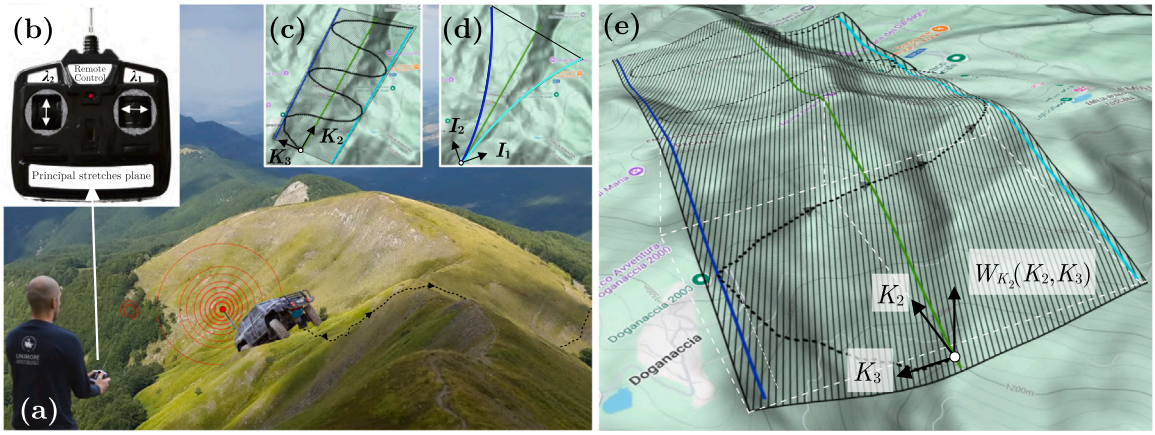

Fig. 2. Analogy between a terrestrial drone topographic survey and the characterization of hyperelastic incompressible materials: (a) mountain surface to be mapped by a drone following the designed dashed path; (b) remote control reference system used by the operator; (c, d) two possible choices of arbitrary reference systems representing the topographic plane; (e) projection of the sinusoidal path (black dashed line) from the topographic plane in (c) onto the mountain surface. (For interpretation of the references to color in this figure legend, the reader is referred to the web version of this article.)

Consequently, the energy or the DEF occupy different domains resulting from different changes of variables that transform stretches into invariants. The surface of the mountain also changes when represented within one of these two distinct invariant domains. In the mechanical characterization, unlike the analogy with a topographic survey, the shape of the mountain depends on the choice of invariants.

Which is the most effective path to gain a comprehensive understanding of the mountain surface using a drone? This question is equivalent to asking which experiment provides the most comprehensive insight into the energy or DEF. Which arbitrary reference system, or corresponding set of invariants, is best suited to represent the mountain?

The invariants domain corresponding to the hatched domains of Figs. 2(c) and (d) are the space $K_2 - K_3$ and the space $I_1 - I_2$, respectively. The DEF for the Criscione (Criscione et al., 2000; Criscione, 2003) invariants are $W_{K_i} = \partial W/\partial K_i$, while for the Cauchy invariants are $W_i = \partial W/\partial I_i$. The associated domains are

$$\underset{K_i}{\mathrm{Dom}}(W_{K_i}) = \{(K_2,\, K_3) \,:\, K_2 \geq 0,\, |K_3| \leq 1\}, \tag{5a}$$

$$\underset{I_i}{\mathrm{Dom}}(W_i) = \left\{(I_1,\, I_2) : \quad \hat{I}_2^{-1}(I_1) \geq I_2 \geq \hat{I}_2(I_1)\right\}, \tag{5b}$$

where the function $\hat{I}_2(I_1)$ is given as

$$\hat{I}_2(I_1) = \frac{9\left(\sqrt{81 - 3I_1^3} + 9\right) - 2\left[\left(\sqrt{81 - 3I_1^3} + 9\right)^{\frac{2}{3}} - \sqrt[3]{-3}I_1\right]^3}{3^{2/3}\sqrt[3]{\sqrt{81 - 3I_1^3} + 9}\left[\left(\sqrt{81 - 3I_1^3} + 9\right)^{\frac{2}{3}} - \sqrt[3]{-3}I_1\right]^2},$$

and $\hat{I}_2^{-1}(I_1)$ is its inverse function shown in Fig. 3(a_2). The image of the Cauchy invariants is bounded between the function $\hat{I}_2$ and its inverse, while the image of the Criscione invariants is bounded between ± 1 (see Figs. 3(a_1) and 3(a_2)). Energy and DEF have a simple and regular domain when expressed in terms of the Criscione invariants (Criscione, 2003; Falope et al., 2024a). In contrast, in the Cauchy invariants space, the change of variable from λ_i to I_i results in a cusp-like shape domain. Inside these domains, the principal stretches are real while outside they assume imaginary or complex values (Currie, 2004).

The drone analogy is thus nearing its limits. The operator of the survey must plan a rational path $\mathcal{P}(I_1, I_2)$ on an arbitrary reference system, just as the experimental investigator must plan a path in the invariant space (step A of Fig. 3). Once the path is planned, the investigator has to map the path $\mathcal{P}(I_1, I_2)$ from the invariant plane to the principal stretches plane where it becomes the (prescribed displacement) path $\mathcal{D}(\lambda_1, \lambda_2)$ (step B). This demonstrates that an unequal biaxial test is sufficient. It is a test with *two independent degrees of freedom* that allows us to travel along any path $\mathcal{D}$ in the principal stretches plane. Finally, once the (unequal) biaxial machine is activated by imposing a displacement history $\mathcal{D}$ corresponding to the principal stretches λ_i, it will be sufficient to measure the reactive nominal stress $\bar{\bar{s}}_i$ and combine them using the relation provided in the next section (step C).

3.2.2. The analytic framework and its rationale

The FFC characterization enhances the standard characterization process outlined in Section 3.1 through two key aspects. First, it aims to map the effective DEF of a hyperelastic isotropic material. Second, it considers the effective domain of the energy and its derivative, thereby providing a well-distributed dataset over the invariant (or principal stretches) domain. The proposed approach is also possible for compressible materials, but using a non-trivial test with three independent kinematic parameters, and replacing the previous figurative example of unknown surfaces with volumes (functions of three variables). For transversely isotropic material, such a procedure is not possible using uniaxial or biaxial tests (Holzapfel and Ogden, 2009). Since to map the DEF it is necessary to be able to sweep along a variable path in the invariants plane, *all you need is an unequal biaxial test*. The importance of the unequal attribute is beyond question.

The equilibrium problem of unequal biaxial homogeneous deformation is solved looking for DEF as unknowns of the problem. Using relations (3), the boundary conditions provide the hydrostatic pressure and the closed-form solution of the DEF,

$$\begin{cases} W_{K_2} = \dfrac{\lambda_1\bar{\bar{s}}_1 \log\lambda_1 + \lambda_2\bar{\bar{s}}_2 \log\lambda_2}{K_2} \\ W_{K_3} = \dfrac{K_2^3\left[\lambda_1\bar{\bar{s}}_1 \log\left(\lambda_1\lambda_2^2\right) - \lambda_2\bar{\bar{s}}_2 \log\left(\lambda_1^2\lambda_2\right)\right]}{3\sqrt{6}\log\left(\frac{\lambda_1}{\lambda_2}\right)\log\left(\lambda_1^2\lambda_2\right)\log\left(\lambda_1\lambda_2^2\right)} \end{cases}, \tag{6a}$$

$$\begin{cases} W_1 = \lambda_1^2\lambda_2^2\,\dfrac{\left(\lambda_1^2\lambda_2^4 - 1\right)\lambda_1^3\bar{\bar{s}}_1 + \left(1 - \lambda_1^4\lambda_2^2\right)\lambda_2^3\bar{\bar{s}}_2}{2\left(\lambda_1^2 - \lambda_2^2\right)\left(\lambda_1^4\lambda_2^2 - 1\right)\left(\lambda_1^2\lambda_2^4 - 1\right)} \\ W_2 = \lambda_1^2\lambda_2^2\,\dfrac{\left(1 - \lambda_1^2\lambda_2^4\right)\lambda_1\bar{\bar{s}}_1 + \left(\lambda_1^4\lambda_2^2 - 1\right)\lambda_2\bar{\bar{s}}_2}{2\left(\lambda_1^2 - \lambda_2^2\right)\left(\lambda_1^4\lambda_2^2 - 1\right)\left(\lambda_1^2\lambda_2^4 - 1\right)} \end{cases}. \tag{6b}$$

Eqs. (6a) and (6b) allow mapping the DEF surfaces, $W_{K_i} = W_{K_i}(K_2, K_3)$ and $W_i = W_i(I_1, I_2)$, since the invariants are functions of the stretches and both stretches and stresses are measurable quantities of the experiments. The coupling between (6) and the corresponding invariants (1) allows us to figure out the shape of the DEF.

The three steps to carry out the FFC characterization of hyperelastic, isotropic, and incompressible solids can be summarized as follows:

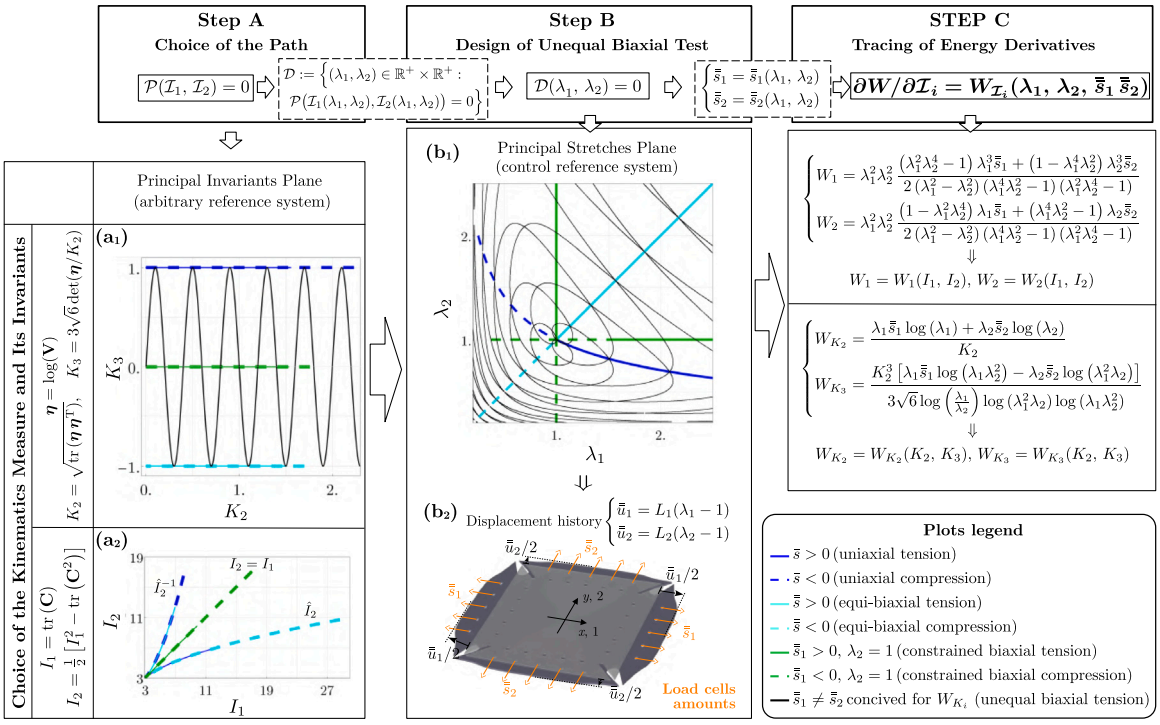

Fig. 3. The three steps of the protocol introduced by the full-field coverage characterization for tracing the derivatives of the energy function, based on the Criscione invariants (K_i) of the Hencky strain tensor $\boldsymbol{\eta}$ and the Cauchy deformation invariants (I_i): step A (left column), choice of a path ($\mathcal{P}$) to generate a well-distributed dataset in the Criscione invariants plane (black lines in the K_2-K_3 plane), along with paths corresponding to standard tests (colored curves); step B (central column), mapping of the path in the invariant plane onto the principal stretches plane, yielding the displacement history ($\mathcal{D}$) used to design unequal biaxial experiments; step C (right column), analytical tools for reconstructing the surface of the derivative of the energy function in the invariants domain. (For interpretation of the references to color in this figure legend, the reader is referred to the web version of this article.)

A Define a path $\mathcal{P}(\mathcal{I}_1, \mathcal{I}_2) = 0$ to be followed in the invariants plane (step A of Fig. 3).

B Map the path from the invariants plane to a corresponding displacement history in the principal stretches plane, $\mathcal{D}(\lambda_1, \lambda_2) = 0$ (step B of Fig. 3), and prescribe the displacement history using the unequal biaxial test.

C Record the nominal stress measured by the load cells ($\bar{s}_1$ and $\bar{s}_2$) during the unequal biaxial test and use these values to compute the DEF using Eqs. (6). Couple the values of DEF with the invariants to reconstruct the DEF surfaces (step C of Fig. 3).

These three steps should be carried out upstream of the standard fitting procedure (see the red dots in Fig. 1). The new approach consolidates the characterization framework by enabling the visualization of the DEF, thus allowing a critical assessment of the energy form adopted in the subsequent fitting procedure.

Two considerations regarding the choice of the invariants and the most common tests used to characterize the materials are essential. The invariants domain depends on the choice of deformation measure and represents the *topographic map* of the energy or DEF surfaces. We opt for the invariants space $K_2 - K_3$ as it has a simpler domain where DEF have a more regular representation than the Cauchy invariant space. The Cauchy invariants space has a cusp-like boundary, near whose apex — where deformations are small — the deformation gradient exhibits a singular experimental behavior (Criscione, 2003; Falope et al., 2024a). When approached in the Cauchy invariants, the uniaxial and equi-biaxial tests are non-exhaustive (Falope et al., 2024a) as they do not yield closed-form solutions of DEF equivalent to relation (6), while DEF are partially exhaustive for the Criscione invariants.

The boundaries of the invariants space K_i and I_i correspond to the paths traveled during uniaxial tensile tests (or equi-biaxial compression) and equi-biaxial tensile tests (or uniaxial compression). This is illustrated in Fig. 3, where blue curves represent uniaxial tests, cyan curves represent equi-biaxial tests, while solid and dashed lines indicate tension and compression, respectively. The simple shear (Rivlin and Saunders, 1951) tests and constrained biaxial tests ($\lambda_1 > 0$, $\lambda_2 = 1$, and $\lambda_3 = 1/\lambda_1$) follow the same path, representing the bisector of both invariants spaces (green curve in Fig. 3). Thus, we confuse the simple shear with the constrained biaxial test. Uniaxial tension is energetically equivalent to equi-biaxial compression as it provides the same information on the DEF. This is due to the same kinematic path $\mathcal{I}_1 - \mathcal{I}_2$ or $\lambda_1 - \lambda_2$. Similarly, equi-biaxial tension corresponds kinematically and energetically to uniaxial compression. Unequal biaxial tests can incorporate all of these experiments, including the simple shear.

Why is material characterization typically performed using only standard experiments along the boundary and bisector paths of the invariants domain? The conventional approaches monitor the mountain by following only the blue, green, or cyan paths shown in Fig. 2. However, are these experimental setups truly optimal? A single unequal biaxial test can encompass the same information content and generate arbitrary paths oscillating within the interior of the domain.

4. A full-field coverage unequal biaxial test

In the present section, we propose a representative path in the invariant plane, $\mathcal{P}(K_2, K_3)$, that produces a well-distributed and dense set of invariants pairs using a single experiment. The corresponding path in the $I_1 - I_2$ space is also reported for comparison. Then, based on the protocol proposed in the previous section, in silico experiments are simulated to compare the capabilities of the FFC characterization and the standard fitting procedure. The comparison focuses on how each method, whether applied to a single or multiple deformation states, can provide the (exact) constitutive parameters of the material used in the in silico simulations.

4.1. Design of an unequal biaxial test

In step A, we propose the following explicit path in the Criscione invariants space:

$$\mathcal{P}(K_2,\, K_3) = K_3 - \sin(\omega_{K_2} K_2) = 0, \tag{7}$$

where ω_{K_2} is the angular frequency of the path. Increasing ω_{K_2} leads to a denser and more refined sampling of the energy and DEF. The black line in Fig. 3(a_1) illustrates the path generated using $\omega_{K_2} = 5\pi$.

In step B, the path (7) is numerically solved in terms of the principal stretches. For unequal biaxial test, the Criscione invariants are given by relation (1a) as

$$K_2 = \sqrt{2}\sqrt{\log\lambda_1 \log\lambda_2 + \log^2\lambda_1 + \log^2\lambda_2},$$
$$K_3 = -\frac{3\sqrt{6}\log\lambda_1 \log\lambda_2 \log(\lambda_1\lambda_2)}{\left[\log^2(\lambda_1\lambda_2) + \log^2\lambda_1 + \log^2\lambda_2\right]^{3/2}},$$

which substitution into (7) provides the following implicit expression for the prescribed displacement history:

$$D(\lambda_1,\, \lambda_2) = \sin\sqrt{2\omega_{K_2}^2\left(\log^2\lambda_1 + \log^2\lambda_2 + \log\lambda_1\log\lambda_2\right)} + \frac{3\sqrt{6}\log\lambda_1\log\lambda_2\log\left(\lambda_1\lambda_2\right)}{\left[\log^2\lambda_1 + \log^2\lambda_2 + \log^2\left(\lambda_1\lambda_2\right)\right]^{3/2}} = 0. \tag{8}$$

This displacement history is an implicit function whose roots define the pairs of principal stretches shown as the black curves in Fig. 3(b_1). Notably, the relationship between the invariants space (7) and the stretches space (8) is not one-to-one: multiple stretch pairs (λ_1, λ_2) correspond to the same point in the invariant plane (K_2, K_3). This redundancy can enhance experimental robustness by providing multiple independent measurements along the same energetic path.

Among the displacement histories shown in Fig. 3(b_1), two independent ones are selected, as illustrated in Fig. 4(a) by the red and magenta curves, path A and path B respectively. Experimentally, these paths correspond to different unequal biaxial tests, or displacement histories, but share the same image $\mathcal{P}(K_2, K_3)$ in the invariants plane of Figs. 4(b) and (c). The corresponding path $\mathcal{P}(I_1, I_2)$ in Fig. 4(c) confirms the ability of the test to uniformly populate the Cauchy invariants domain as well. Note that the definition of $\mathcal{P}(I_1, I_2)$ in the space of Cauchy invariants is possible in terms of implicit representation only. This aspect, in addition to the reasons reported by Neff et al. (2015), supports the choice of the Criscione invariants or the use of the Hencky strain as the deformation measure. Given a biaxial machine and a rectangular sheet of soft material with sides L_1 and L_2, the operator can now program two prescribed displacement histories — associated to the two independent actuators of the machine — along directions 1 and 2 of Fig. 3(b_2) given as $\bar{\bar{u}}_1 = L_1(\lambda_1 - 1)$ and $\bar{\bar{u}}_2 = L_2(\lambda_2 - 1)$.

In step C, the experimental operator couples the stresses $\bar{\bar{s}}_1$ and $\bar{\bar{s}}_2$ (monitored by the load cells) with the principal invariants (1) and traces the effective DEF of the material using relations (6). An appropriate energy form exhibiting the required nonlinearities can now be selected (see point 0 in Fig. 1). In addition, the density of the experimental data acquired allows for a fitting procedure that full-field covers the energy domain (see point (1–2) in Fig. 1).

The path B, shown as the magenta displacement history in Fig. 4(a), must be excluded because it falls within an experimentally inaccessible region (EIR) for the following reason. For $\lambda_1 < 1$, any path lying below the uniaxial compression curve ($\lambda_1^{-1/2}$) in Fig. 4(d) requires simultaneous compression along direction 1 and direction 2. This condition defines an EIR due to the practical challenges of applying such a loading state while ensuring homogeneous deformations. However, the darker gray region, named EIR 1 in Fig. 4(d), is also an EIR. This region corresponds to a transition between the uniaxial compression ($\bar{s}_1 < 0$ and $\bar{s}_2 = 0$) and an unequal biaxial stress configuration in which the applied stresses have opposite signs ($\bar{\bar{s}}_1 < 0$ and $\bar{\bar{s}}_2 > 0$), which is also not experimentally feasible. Since the unequal biaxial experiment is symmetric with respect to the stretches, also the symmetric part of EIR 1, that is EIR 2, must be discarded. This explains the experimental inaccessibility of the magenta path.

Looking at Figs. 4(a) and (b), it is not surprising that the curves λ_1^{-2} and λ_1 have the same image in the invariants domain. The transition points between successive load branches — from (*ii*) to (*iii*) and from (*iv*) to (*v*) — along paths A and B in Fig. 4(a) share the same image in the invariants plane, corresponding to the minima of the sinusoidal path shown in Fig. 4(b). This is justified by the same eigenvalues that these states of deformations possess, which differ for a permutation of the stretches only. Indeed, for incompressible materials, the equibiaxial test is characterized by the eigenvalues $(\lambda_1, \lambda_1, \lambda_1^{-2})$, while the curve λ_1^{-2} is identified by the eigenvalues $(\lambda_1, \lambda_1^{-2}, \lambda_1)$. For isotropic and incompressible material, these curves are associated with the same invariants, namely, have the same image in the invariant domain. The symmetric counterpart of path A with respect to λ_1 is also a permutation of the stretches, and therefore conveys the same information from an energetic point of view. The only region that must be investigated for the FFC characterization of isotropic and incompressible materials is the one swept out by the path A in Fig. 4(d).

Before providing an application case, several analytical assumptions must be experimentally satisfied to ensure the validity of the method: the deformation should remain homogeneous throughout the sample; the stretches employed in the computation must correspond to the effective ones; the material should be hyperelastic and incompressible, or at least nearly incompressible.

The homogeneous nature of the deformation must be verified or critically discussed. In biaxial tests, deformations are generally considered homogeneous far from the anchor zones of the sample (Pancheri and Dorfmann, 2014; Seibert et al., 2014; Fujikawa et al., 2014; Hartmann et al., 2018; Potter et al., 2018; Jiang et al., 2021; Falope et al., 2024a; Havasi and Kossa, 2025; Zhang et al., 2025). Inhomogeneous deformations can cause the prescribed stretch to differ significantly from the effective stretch, especially at high deformation values. This highlights the importance of optical monitoring (Sasso et al., 2008; Malcolm et al., 2002) in accurately capturing the true stretches of the sample.

The incompressibility of the material must be checked or at least discussed (Giannakopoulos and Triantafyllou, 2007; Falope et al., 2025). Three-dimensional full-field monitoring of both faces of the specimen is essential (Davis et al., 2017; Rossi et al., 2018; Falope et al., 2024b), not only for the redundancy of the in-plane stretches but also for the acquisition of the out-of-plane stretch. The discrepancy between the out-plane stretch λ_3 and the incompressibility condition derived from the in-plane stretches, $1/\lambda_1\lambda_2$, can be used to define an incompressibility index.

The assumption of Green elastic behavior must be experimentally verified or at least systematically monitored (Bogoslovov et al., 2007; Zhang et al., 2009). Different displacement histories leading to the same path $\mathcal{P}(I_1, I_2)$ can be employed as loading–unloading cycles to traverse the invariants plane in both forward and reverse directions. If the material exhibits hyperelastic behavior, the loading and unloading trajectories should overlap. In contrast, the presence of inelastic effects can be identified by deviations between loading and unloading paths, potentially allowing for the experimental delineation of inelastic domains in the invariants space.

In addition to the basic assumptions that must be verified for the proper application of the FFC protocol, there are strongly nonlinear material behaviors that should be excluded, as they could compromise the validity of the procedure. Such behaviors, including rate dependence, anisotropy, and evolving microstructure, may lead to misleading parameter identification if present. A careful preliminary assessment of the material is therefore necessary to ensure that these effects are negligible or appropriately accounted for before applying the FFC characterization.

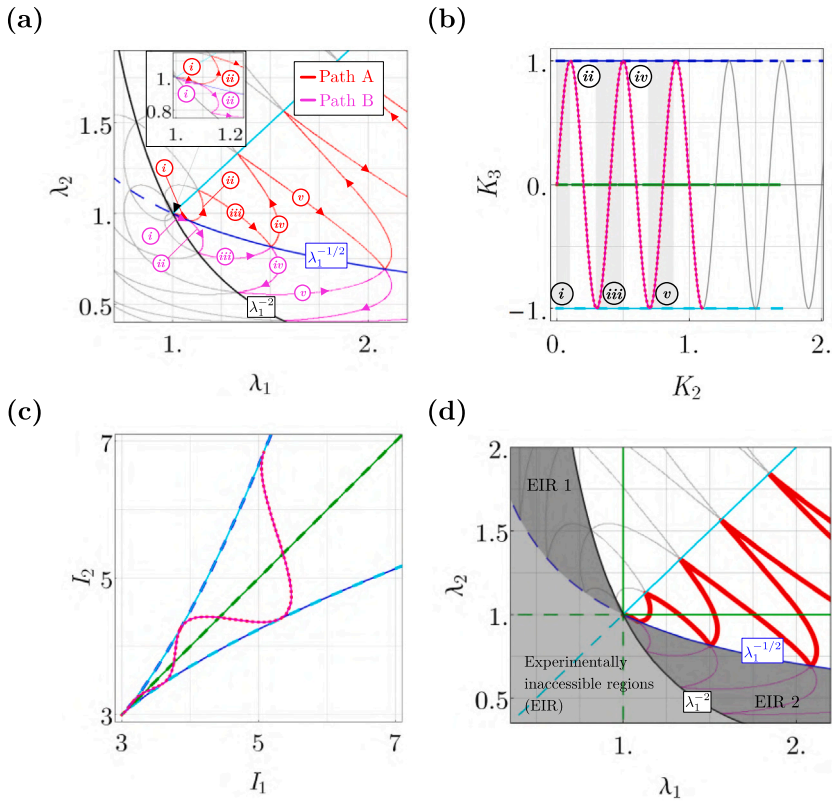

Fig. 4. Application of the protocol of the full-field coverage (FFC) characterization: (a) two displacement histories $\mathcal{D}(\lambda_1, \lambda_2)$, namely path A (red) and path B (magenta), obtained as numerical solutions of Eq. (8), both yielding the same path in the invariants domain; (b) path $\mathcal{P}(K_2, K_3)$ from Eq. (7), shown in the Criscione invariants domain and corresponding to the displacement histories in sub-figure (a), where the first five branches are labeled with Greek numerals ((*i*)–(*v*)); (c) path $\mathcal{P}(I_1, I_2)$, also from Eq. (7), shown in the Cauchy invariants domain and corresponding to the displacement histories in sub-figure (a); (d) final selected displacement history $\mathcal{D}(\lambda_1, \lambda_2)$ (red curve) along with the experimentally inaccessible regions (EIR), where tests cannot be performed using standard a biaxial device. EIR1 and EIR2 are symmetric with respect to the equi-biaxial path. (For interpretation of the references to color in this figure legend, the reader is referred to the web version of this article.)

4.2. Evidence from in silico simulations

In this section, contrary to the usual approach, we assume that the form of the strain energy function and its constitutive parameters are known. The finite element (FE) software COMSOL Multiphysics 6.1® is used to simulate several states of homogeneous deformation. Specifically, we simulate uniaxial tension (UX), equi-biaxial tension (EBX), constrained biaxial tension (CBX), and unequal biaxial (UNBX) tension along the path A introduced in the previous section. The results are treated as those of an experimentally tested material with a known energy function and constitutive parameters. The objective is to assess which procedure — either the standard fitting method or the FFC characterization — yields constitutive parameters values that are closest to the exact ones.

We chose the following generalization of the Pucci-Saccomandi model (Pucci and Saccomandi, 2002) as reference strain energy function (Anssari-Benam, 2024):

$$W(I_1, I_2) = \frac{3(n-1)\mu N}{2n}\left[\frac{I_1-3}{3(n-1)N} - \log\frac{I_1-3N}{3(1-N)}\right] + C_2\frac{3(m-1)}{m}\left[\frac{I_2-3}{3(m-1)} + \log\frac{I_2}{3}\right], \tag{9}$$

and we assume as exact constitutive parameters $\mu = 0.27$, $N = 25.37$, $n = 2.83$, $C_2 = 0.04$, and $m = 20.17$. These values were obtained by Anssari-Benam (2024) by fitting the experimental data of Treloar (1944). The choice of this energy form is motivated by its high number of degrees of freedom — specifically, the five constitutive parameters — which enhance the widely used Pucci-Saccomandi models by introducing a stronger dependence on the second invariant of the deformation.

Using the FE code, we simulated four stress states: uniaxial tension, equi-biaxial tension, constrained biaxial tension, and unequal biaxial tension. The FE simulations are performed by modeling a rectangular hyperelastic block using the strain energy function defined in Eq. (9), implemented as a user-defined hyperelastic material. Depending on the state of deformation investigated, prescribed displacements are applied to the lateral surfaces of the solid, ensuring homogeneous deformations. All simulations are conducted under displacement control. Since the deformation is homogeneous, the mesh does not influence the results. Quadratic Lagrangian shape functions are used. Thus, the FE solver provides the exact solution of the problem.

To make the in silico simulations more representative of experimental data, and to distinguish them from the exact solution of the FE model (s_i^{FE}), random noise was added to the FE stresses. The noise is defined as a function of the scalar quantity $\Lambda = \left(\lambda_1^2 + \lambda_2^2 + \lambda_1^{-2}\lambda_2^{-2}\right)^{1/2}/\sqrt{3}$, which represents the norm of the stretch vector. The experimental noise is assumed to follow a normal distribution $\mathcal{N}(\Lambda)$, with unitary mean value and a variance of 0.5, further scaled by a random variable $\mathscr{R} \in [-0.5, +0.5]$. The choice of the distribution and its parameters is based on the analysis and fitting of typical experimental errors reported in the literature (Anssari-Benam and Horgan, 2022; Falope et al., 2025). As a result, the stress values used in the fitting procedure are modified according to

$$s_i(\lambda_1, \lambda_2) = s_i^{\mathrm{FE}}\left[1 + \mathscr{R}\,\mathcal{N}(\Lambda)\right]. \tag{10}$$

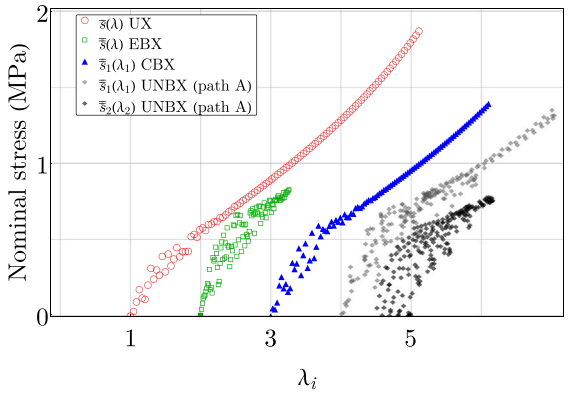

Fig. 5. Stress vs. stretch curves obtained from in silico experiments performed with COMSOL Multiphysics, using the energy form (9) (Anssari-Benam, 2024), relation (10), and the constitutive parameters $\mu = 0.27$, $N = 25.37$, $n = 2.83$, $C_2 = 0.04$, and $m = 20.17$: uniaxial tension (UX), equi-biaxial tension (EBX), constrained biaxial tension (CBX), and unequal biaxial test following path A (red path in Fig. 4). Curves have been shifted by one unit of stretch for clarity. (For interpretation of the references to color in this figure legend, the reader is referred to the web version of this article.)

The nominal stresses used for the standard fitting and FFC characterization procedures are shown in Fig. 5, with the curves horizontally shifted by one unit of stretch for clarity.

All sets of constitutive parameters obtained from the standard fitting of single tests reported in Table 1, as well as from the FFC characterization and the simultaneous fitting of multiple tests, yield an excellent description of the response function (see Fig. 6(a)). For the best-fit parameters obtained from single tests and UNBX, Figs. 6(b) and (c) illustrate the quality of the fits in terms of the relative error ϵ_r, calculated with respect to the nominal stresses predicted using the exact constitutive parameters. All relative errors were found to be negligible. However, our objective goes beyond reproducing only the stress response. We aim to establish a robust procedure for reliably identifying the exact values of the constitutive parameters. This approach is intended to mitigate the issue of non-uniqueness in parameter identification, as discussed by Ogden et al. (2004).

The standard fitting procedure for single tests is first performed using the NRMSE associated with the nominal stress–stretch curve.[3] The results are reported in Table 1 in terms of constitutive parameters and relative errors.

Among the single test cases, only the UNBX test following path A yields constitutive parameter values with acceptable relative errors below 38%. The results of the simultaneous fitting of multiple tests, where the objective function is defined as the sum of the individual NRMSE values, are shown in Table 2. An exception is the last column, which refers to the UNBX test along path A, including the unloading phase following the CBX kinematic path (see Fig. 6(d)). This corresponds to path A in Fig. 4(d), which, upon its intersection with the green curve representing the CBX path, follows the horizontal segment during an unloading phase back to the origin. The UNBX test is capable of incorporating any biaxial loading or unloading condition. It is observed that in the case of a proper real experiment, the inclusion of an unloading path makes it possible to validate the Green elastic assumption.

Table 2 shows that the reliability of the fitting procedure significantly improves when multiple experiments are used. However, the UNBX test unloaded along the CBX path is the best choice introduced by the FFC characterization. Let $\boldsymbol{\epsilon}_{r,\mathbf{p}}$ be the vector of relative errors of the estimated constitutive parameters $\mathbf{p}$. We introduce its Euclidean norm, $\|\boldsymbol{\epsilon}_{r,\mathbf{p}}\|$, as a reliability measure of single or multiple tests in returning the exact values of the constitutive parameters. Fig. 6(e) shows that it is more convenient to use a single UNBX test following path A, which ends with an unloading branch that follows the CBX test, rather than the simultaneous fitting of the standard experiments (UX+EBX+CBX).

Table 1
Exact values of the constitutive parameters (second column) of the model defined in Eq. (9), and values obtained via the standard fitting procedure on single tests (central columns): uniaxial (UX), equi-biaxial (EBX), constrained biaxial (CBX), and unequal biaxial (UNBX) along path A (red path in Fig. 4), which is the only test providing full-field coverage of the entire stretch domain. Relative errors with respect to the exact values are reported in brackets.

Const.	Exact	Standard fitting procedure on a single test			Full-field coverage characterization
param.	values	UX	EBX	CBX	UNBX path A
μ	0.27	0.263 (2%)	0.328 (−21%)	0.264 (2%)	0.273 (−1%)
N	25.37	31.94 (−25%)	666.52 (−2527%)	32.52 (−28%)	19.82 (21%)
n	2.83	47.45 (−1576%)	49.62 (−1653%)	66.41 (−2246%)	1.75 (38%)
C_2	0.04	0.051 (−26%)	0.025 (37%)	0.045 (−13%)	0.041 (−1%)
m	20.17	44.34 (−119%)	65.86 (−226%)	33.02 (−63%)	22.13 (−9%)

5. Discussion

The proposed protocol for the FFC characterization (Figs. 1 and 3) represents a shift toward a more comprehensive approach to the material characterization. It justifies the selection of the experimental dataset based on a solid analytical rationale. Despite the widespread use of uniaxial, equi-biaxial, and shear tests,[4] often motivated by experimental simplicity, it is important to critically assess whether such tests alone provide a sufficiently complete description of the material energy function or its derivatives. The intent is to establish a method that reduces the variability in the values assumed by the constitutive parameters. In the case of real experimental data — as opposed to in silico simulations — the ability to visualize the DEF and fit them directly could further enhance the potential and robustness of the proposed method.

The proposed FFC approach enables a controlled sampling across the invariant domain, offering a denser and more representative dataset that strengthens subsequent data-driven or path-dependent analyses. This mitigates the issues of sparse data and extrapolation that typically arise when constitutive parameters are identified from conventional tests. For instance, identifying parameters from a single test — such as a constrained biaxial or a simple shear test lying along the bisector of the invariant plane — yields parameters that fit that particular loading path well but rely on the extrapolation of energy insight to describe other deformation states. Conversely, identifying parameters from two tests along the boundaries of the invariant domain — such as pure tension and pure compression — provides a good fit along those boundaries, yet the material response for intermediate states must be interpolated between these two edges. In this case, it is observed that the distance

[3] For the fitting procedure, performed on both single and multiple tests using the *fmincon* function of Matlab®, the same upper and lower bounds are used for the constitutive parameters, as well as the same settings of the Matlab code.

[4] We recall that the kinematics of simple shear and constrained biaxial tests are equivalent, as they share the same principal stretches. By contrast, the kinematics of *angular shear deformations* (Falope et al., 2026) differs substantially.

Table 2
Exact values of the constitutive parameters (second column) of the model defined in Eq. (9), and values obtained via the standard fitting procedure on multiple tests (central columns): uniaxial (UX), equi-biaxial (EBX), constrained biaxial (CBX), and unequal biaxial (UNBX) along path A (red path in Fig. 4), which ends with an unloading phase along the CBX path. Among the various combinations of multiple tests, UNBX is the only single test also included on its own. Relative errors with respect to the exact values are reported in brackets.

Const.	Exact	Simultaneous fitting procedure of multiple tests			Full-field coverage characterization
param.	values	UX+EBX	EBX+CBX	UX+EBX+CBX	UNBX path A unloaded along CBX
μ	0.27	0.266 (1.57%)	0.262 (2.83%)	0.269 (0.43%)	0.27 (−0.07%)
N	25.37	28.47 (−12%)	31.98 (−26%)	26.1 (−2%)	25.09 (1%)
n	2.83	5.19 (−83%)	58.26 (−1958%)	3.17 (−12%)	2.73 (3%)
C_2	0.04	0.047 (−18.31%)	0.047 (−17.88%)	0.042 (−4.38%)	0.04 (0.35%)
m	20.17	32.28 (−60%)	25.26 (−25%)	23.31 (−15%)	19.77 (1.97%)

between interpolation points at the boundary corresponds to $K_3 = 2$ (in the Criscione formulation), whereas for Cauchy invariants this distance varies and increases with the level of deformation (see Figs. 3(a_1) and 3(a_2)). By contrast, the proposed unequal biaxial test allows control over the position and spacing of the interpolation points, thus generating a denser and more continuous sampling of the invariants or stretches domain and eliminating the need for extrapolation. The proposed procedure should be regarded as complementary and provides a foundational dataset upon which data-driven approaches can be built. In addition, by enabling a variety of tests that follow similar deformation paths, it can support the study of inelastic effects and the exploration of path-dependent material responses.

Recalling the analogy of the drone survey of Fig. 2, if we saw the drone operator monitoring the surface of a mountain, focusing only on the boundary paths or the bisector path, what advice would we give? The analogy of a drone operator guiding the drone along only the boundary or bisector paths (as illustrated in Fig. 2) highlights the limitations of conventional testing approaches. A broader exploration of the invariants space, enabled by a well-conceived unequal biaxial test, allows for richer and more representative sampling of the material constitutive behavior. To trace the real-material response functions and to carry out a full-field coverage characterization, *all you need is a well-conceived unequal biaxial test*, whose unloading path follows the constrained biaxial test (Fig. 6(d)).

6. Conclusions

The standard mechanical characterization process of hyperelastic, isotropic, and incompressible materials has been enhanced by introducing the full-field coverage (FFC) characterization over the entire energy domain.

An experiment can be considered suitable and reliable for the mechanical characterization of a material if, first, it is well distributed over the energy domain — whether in terms of stretches or invariants — and second, if it allows for the tracing of the energy derivatives. Thus, we have analyzed the kinematic paths of the most commonly used experiments within the space of principal stretches or deformation invariants. This analysis has allowed us to demonstrate two main outcomes. First, it is not necessary to explore the entire stretch domain to capture the derivatives of the energy function. Certain paths, although differing in the stretch space due to permutations of the principal stretches, map to the same trajectory in the invariant space. Such paths are therefore energetically equivalent. Second, we have shown that the proposed unequal biaxial test, which follows a constrained biaxial kinematic path during the unloading phase (Fig. 6(d)), is the most reliable and suitable experiment for identifying the constitutive parameters of the material. The full-field characterization performed in this test reduces the variability of the identified parameters.

After presenting the analytical foundations, the rationale of the two main outcomes has been introduced through the analogy of a survey of a mountain relief carried out by an operator using a terrestrial drone. This figurative example highlights two limitations of the standard fitting process: the inability of standard experiments to allow for tracing the derivatives of the strain energy, and the failure of the kinematics of standard experiments to sweep within the energy domain. Through in silico simulations of different experiments, characterized by known constitutive parameters, we conducted the fitting procedure according to the standard characterization process and according to the full-field coverage characterization. The results have demonstrated that a single test alone provides a more robust experimental dataset than the simultaneous fitting of three different tests. *All you need is an unequal biaxial test.*

Declaration of competing interest

The authors declare that they have no known competing financial interests or personal relationships that could have appeared to influence the work reported in this paper.

Acknowledgments

The author gratefully acknowledges financial support from the Italian Ministry of Research (MUR) through the research grant FIS 2 "Large and offshore deformations of everyday life: from seismic isolators to person's health" (proj. FIS-2023-01661, CUP E53C25000450001). Financial support by the National Group of Mathematical Physics (GNFM-INdAM) is also acknowledged.

Data availability

Data will be made available on request.

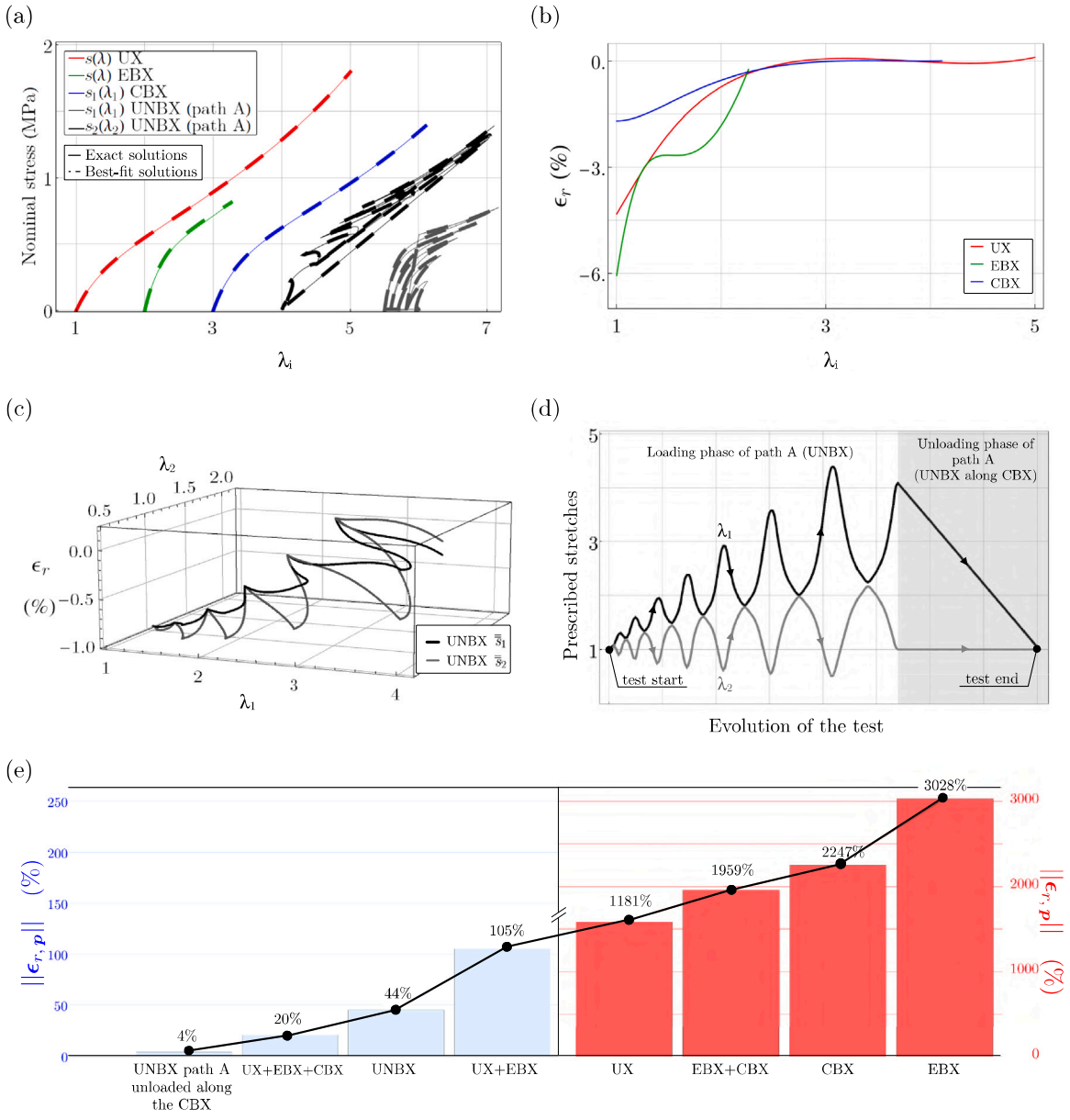

Fig. 6. Outcomes of the fitting procedure: (a) comparison between the nominal stresses of the single tests shown as exact solutions (solid lines) and the best-fit solutions (dashed lines). The exact solutions are obtained using the exact constitutive parameters, whereas the best-fit ones are computed using the parameters reported in Table 1; (b) relative errors of the nominal stress between the exact solution and the best-fit solution for uniaxial (UX), equi-biaxial (EBX), and constrained biaxial (CBX) tests; (c) relative errors of the nominal stresses for the unequal biaxial (UNBX) path A; (d) prescribed stretches for the proposed unequal biaxial path A, combined with an unloading phase following the constrained biaxial (CBX) path; (e) fitting score expressed as the norm of the vector of relative errors on the constitutive parameters, considering the model defined in Eq. (9) and the exact parameter values: $\mu = 0.27$, $N = 25.37$, $n = 2.83$, $C_2 = 0.04$, and $m = 20.17$ (blue bars correspond to the left axis; red bars to the right axis). (For interpretation of the references to color in this figure legend, the reader is referred to the web version of this article.)

References

Anssari-Benam, A., 2024. A generalisation of the Pucci–Saccomandi model of rubber elasticity. Int. J. Non-Linear Mech. 158, 104578. http://dx.doi.org/10.1016/j.ijnonlinmec.2023.104578.

Anssari-Benam, A., Goriely, A., Saccomandi, G., 2024. Generalised invariants and pseudo-universal relationships for hyperelastic materials: A new approach to constitutive modelling. J. Mech. Phys. Solids 193, 105883. http://dx.doi.org/10.1016/j.jmps.2024.105883.

Anssari-Benam, A., Horgan, C.O., 2022. A three-parameter structurally motivated robust constitutive model for isotropic incompressible unfilled and filled rubber-like materials. Eur. J. Mech. A Solids 95, 104605. http://dx.doi.org/10.1016/j.euromechsol.2022.104605.

Baker, M., Ericksen, J.L., 1954. Inequalities restricting the form of the stress-deformation relations for isotropic elastic solids and Reiner Rivlin fluids. J. Wash. Acad. Sci. 44, 33–35.

Beatty, M.F., 1987. Topics in finite elasticity: Hyperelasticity of rubber, elastomers, and biological tissues with examples. Appl. Mech. Rev. 40, 1699–1734. http://dx.doi.org/10.1115/1.3149545.

Bogoslovov, R.B., Roland, C.M., Gamache, R.M., 2007. Impact-induced glass transition in elastomeric coatings. Appl. Phys. Lett. 90, http://dx.doi.org/10.1063/1.2745212.

Brieu, M., Diani, J., Bhatnagar, N., 2007. A new biaxial tension test fixture for uniaxial testing machine—A validation for hyperelastic behavior of rubber-like materials. J. Test. Eval. 35, 364–372. http://dx.doi.org/10.1520/JTE100688.

Costecalde, L., Leygue, A., Coret, M., Verron, E., 2023. Data-driven identification of hyperelastic models by measuring the strain energy density field. Rubber Chem. Technol. 96, 443–454. http://dx.doi.org/10.5254/rct-23.386903.

Criscione, J.C., 2003. Rivlin's representation formula is ill-conceived for the determination of response functions via biaxial testing. J. Elasticity 70, 129–147. http://dx.doi.org/10.1023/B:ELAS.0000005586.01024.95.

Criscione, J.C., Humphrey, J.D., Douglas, A.S., Hunter, W.C., 2000. An invariant basis for natural strain which yields orthogonal stress response terms in isotropic hyperelasticity. J. Mech. Phys. Solids 48, 2445–2465. http://dx.doi.org/10.1016/S0022-5096(00)00023-5.

Crocker, L.E., Duncan, B.C., Hughes, R.G., Urquhart, J.M., 1999. Hyperelastic Modelling of Flexible Adhesives. NPL Report CMMT(A)183, National Physical Laboratory (NPL), Teddington, UK, PAJ1 Report No 14, May 1999.

Currie, P.K., 2004. The attainable region of strain-invariant space for elastic materials. Int. J. Non-Linear Mech. 39, 833–842. http://dx.doi.org/10.1016/S0020-7462(03)00059-3.

Currie, P.K., 2005. Comparison of incompressible elastic strain energy functions over the attainable region of invariant space. Math. Mech. Solids 10, 559–574. http://dx.doi.org/10.1177/1081286505036420.

Davis, F., L'Hommel, J., Le Cam, J.-B., Pierron, F., 2017. Quantification of the compressibility of elastomers using DIC. In: International Digital Imaging Correlation Society: Proceedings of the First Annual Conference, 2016. Springer, pp. 199–201. http://dx.doi.org/10.1007/978-3-319-51439-0_47.

Falope, F.O., Lanzoni, L., Tarantino, A.M., 2024a. Energetic exhaustiveness for the direct characterization of energy forms of hyperelastic isotropic materials. J. Mech. Phys. Solids 193, 105885. http://dx.doi.org/10.1016/j.jmps.2024.105885.

Falope, F.O., Lanzoni, L., Tarantino, A.M., 2024b. Lateral buckling of the compressed edge of a beam under finite bending. Eur. J. Mech. A Solids 107, 105373. http://dx.doi.org/10.1016/j.euromechsol.2024.105373.

Falope, F.O., Lanzoni, L., Tarantino, A.M., 2025. Experiments on the finite torsion of nearly incompressible rubber-like materials: Nonlinear effects, analytic modeling and rubber characterization. Internat. J. Engrg. Sci. 211, 104254. http://dx.doi.org/10.1016/j.ijengsci.2025.104254.

Falope, F.O., Lanzoni, L., Tarantino, A.M., 2026. Shear models in finite elasticity. J. Elasticity 158, 12. http://dx.doi.org/10.1007/s10659-026-10187-3.

Fujikawa, M., Maeda, N., Yamabe, J., Kodama, Y., Koishi, M., 2014. Determining stress–strain in rubber with in-plane biaxial tensile tester. Exp. Mech. 54, 1639–1649. http://dx.doi.org/10.1007/s11340-014-9942-7.

Giannakopoulos, A.E., Triantafyllou, A., 2007. Spherical indentation of incompressible rubber-like materials. J. Mech. Phys. Solids 55, 1196–1211. http://dx.doi.org/10.1016/j.jmps.2006.11.010.

Hartmann, S., Gilbert, R.R., Sguazzo, C., 2018. Basic studies in biaxial tensile tests. GAMM-Mitt. 41, e201800004. http://dx.doi.org/10.1002/gamm.201800004.

Havasi, K., Kossa, A., 2025. A novel approach to calculating the equibiaxial stress response from biaxial tests with non-homogeneous deformations. J. Strain Anal. Eng. Des. 03093247241312393. http://dx.doi.org/10.1177/03093247241312393.

Holzapfel, G.A., Ogden, R.W., 2009. On planar biaxial tests for anisotropic nonlinearly elastic solids. a continuum mechanical framework. Math. Mech. Solids 14, 474–489. http://dx.doi.org/10.1177/1081286507084411.

Horgan, C.O., Murphy, J.G., 2025. Some remarks on the principal stretch versus invariant formulation for constitutive modeling of incompressible isotropic hyperelastic materials. J. Elasticity 157, 50. http://dx.doi.org/10.1007/s10659-025-10142-8.

Jiang, M., Sridhar, R.L., Robbins, A.B., Freed, A.D., Moreno, M.R., 2021. A versatile biaxial testing platform for soft tissues. J. Mech. Behav. Biomed. Mater. 114, 104144. http://dx.doi.org/10.1016/j.jmbbm.2020.104144.

Kulwant, V., Arvind, K., Prasad, D., Sreejith, P., Mohankumar, K.V., Kannan, K., 2023. A semi-analytical inverse method to obtain the hyperelastic potential using experimental data. J. Mech. Phys. Solids 181, 105431. http://dx.doi.org/10.1016/j.jmps.2023.105431.

Leygue, A., Coret, M., Réthoré, J., Stainier, L., Verron, E., 2018. Data-based derivation of material response. Comput. Methods Appl. Mech. Engrg. 331, 184–196. http://dx.doi.org/10.1016/j.cma.2017.11.013.

Malcolm, D.T.K., Nielsen, P.M.F., Hunter, P.J., Charette, P.G., 2002. Strain measurement in biaxially loaded inhomogeneous, anisotropic elastic membranes. Biomech. Model. Mechanobiol. 1, 197–210. http://dx.doi.org/10.1007/s10237-002-0018-8.

Meunier, L., Chagnon, G., Favier, D., Orgéas, L., Vacher, P., 2008. Mechanical experimental characterisation and numerical modelling of an unfilled silicone rubber. Polym. Test. 27, 765–777. http://dx.doi.org/10.1016/j.polymertesting.2008.05.011.

Neff, P., Ghiba, I.-D., Lankeit, J., 2015. The exponentiated hencky-logarithmic strain energy. Part I: Constitutive issues and rank-one convexity. J. Elasticity 121, 143–234. http://dx.doi.org/10.1007/s10659-015-9524-7.

Ogden, R.W., 1972. Large deformation isotropic elasticity–on the correlation of theory and experiment for incompressible rubberlike solids. Proc. R. Soc. A 326, 565–584. http://dx.doi.org/10.1098/rspa.1972.0026.

Ogden, R.W., Saccomandi, G., Sgura, I., 2004. Fitting hyperelastic models to experimental data. Comput. Mech. 34, 484–502. http://dx.doi.org/10.1007/s00466-004-0593-y.

Pancheri, F.Q., Dorfmann, L., 2014. Strain-controlled biaxial tension of natural rubber: New experimental data. Rubber Chem. Technol. 87, 120–138. http://dx.doi.org/10.5254/rct.13.87902.

Potter, S., Graves, J., Drach, B., Leahy, T., Hammel, C., Feng, Y., Baker, A., Sacks, M.S., 2018. A novel small-specimen planar biaxial testing system with full in-plane deformation control. J. Biomech. Eng. 140, 051001. http://dx.doi.org/10.1115/1.4038779.

Prasad, D., Kannan, K., 2020. An analysis driven construction of distortional-mode-dependent and hill-stable elastic potential with application to human brain tissue. J. Mech. Phys. Solids 134, 103752. http://dx.doi.org/10.1016/j.jmps.2019.103752.

Pucci, E., Saccomandi, G., 2002. A note on the Gent model for rubber-like materials. Rubber Chem. Technol. 75, 839–852. http://dx.doi.org/10.5254/1.3547687.

Rivlin, R.S., 2004. A note on the constitutive equation for an isotropic elastic material. Math. Mech. Solids 9, 121–129. http://dx.doi.org/10.1177/1081286504042588.

Rivlin, R.S., Saunders, 1951. Large elastic deformations of isotropic materials VII. Experiments on the deformation of rubber. Philos. Trans. R. Soc. Lond. Ser. A, Math. Phys. Sci. 243, 251–288. http://dx.doi.org/10.1098/rsta.1951.0004.

Rivlin, R.S., Sawyers, K.N., 1976. The strain-energy function for elastomers. Trans. Soc. Rheol. 20, 545–557. http://dx.doi.org/10.1122/1.549436.

Rossi, M., Cortese, L., Genovese, K., Lattanzi, A., Nalli, F., Pierron, F., 2018. Evaluation of volume deformation from surface DIC measurement. Exp. Mech. 58, 1181–1194. http://dx.doi.org/10.1007/s11340-018-0409-0.

Sasso, M., Palmieri, G., Chiappini, G., Amodio, D., 2008. Characterization of hyperelastic rubber-like materials by biaxial and uniaxial stretching tests based on optical methods. Polym. Test. 27, 995–1004. http://dx.doi.org/10.1016/j.polymertesting.2008.09.001.

Seibert, H., Scheffer, T., Diebels, S., 2014. Biaxial testing of elastomers: Experimental setup, measurement and experimental optimisation of specimen's shape. Tech. Mech.-Eur. J. Eng. Mech. 34, 72–89. http://dx.doi.org/10.24352/UB.OVGU-2017-054.

Signorini, A., 1930. Sulle deformazioni termoelastiche finite. In: Proc. 3rd Int. Congr. Appl. Mech. 2, 8G-89.

Signorini, A., 1959. Questioni di elasticità non linearizzata. Rend. Mat. Appl. 18, 95–139.

Steinmann, P., Hossain, M., Possart, G., 2012. Hyperelastic models for rubber-like materials: Consistent tangent operators and suitability for Treloar's data. Arch. Appl. Mech. 82, 1183–1217. http://dx.doi.org/10.1007/s00419-012-0610-z.

Treloar, L.R.G., 1944. Stress-strain data for vulcanized rubber under various types of deformation. Rubber Chem. Technol. 17, 813–825. http://dx.doi.org/10.1039/TF9444000059.

Truesdell, C., 1952. The mechanical foundations of elasticity and fluid dynamics. J. Ration. Mech. Anal. 1, 125–300.

Truesdell, C., 1956. Das ungelöste hauptproblem der endlichen elastizitätstheorie. ZAMM Z. Angew. Math. Mech. 36, 97–103. http://dx.doi.org/10.1002/zamm.19560360304.

Zhang, Q., Liu, L., Zhang, L., Li, F., 2025. How to effectively perform equibiaxial tension for rubber materials? Polymer 324, 128256. http://dx.doi.org/10.1016/j.polymer.2025.128256.

Zhang, H.P., Niemczura, J., Dennis, G., Ravi-Chandar, K., Marder, M., 2009. Toughening effect of strain-induced crystallites in natural rubber. Phys. Rev. Lett. 102, 245503. http://dx.doi.org/10.1103/PhysRevLett.102.245503.